IEEE Access
Multidisciplinary ⋮ Rapid Review ⋮ Open Access Journal

Received July 6, 2021, accepted July 15, 2021, date of publication July 19, 2021, date of current version July 27, 2021.

Digital Object Identifier 10.1109/ACCESS.2021.3098416

NLOS Identification Based UWB and PDR Hybrid Positioning System

DAE-HO KIM AND JAE-YOUNG PYUN
Department of Information and Communication Engineering, Chosun University, Gwangju 61452, South Korea
Corresponding author: Jae-Young Pyun (jypyun@chosun.ac.kr)

This work was supported by the Research Fund from Chosun University, in 2020.

ABSTRACT Some of the researches on indoor positioning have been conducted, but there are still many constraints on indoor positioning approaches. Among these approaches, ultra-wideband (UWB) provides a fast and precise positioning performance but requires a sufficient infrastructure and a clear line-of-sight (LOS) channel. However, inertial sensor-based pedestrian dead reckoning (PDR) operates without infrastructure, but it requires position initialization and has error drift problems. In this study, we propose a hybrid positioning system that fully combines UWB and PDR to overcome such constraints and improve the positioning performance. This hybrid positioning system uses a Kalman filter (KF) based fusion method that identifies non-line-of-sight (NLOS) environments and mitigates UWB errors through PDR. We also evaluated the proposed system implemented using practical testbed devices at indoor environments classified as LOS, weak NLOS, and hard NLOS. The evaluation results showed that the proposed system significantly improves the positioning performance and alleviates the positioning constraints, as compared to the single positioning system. Our system has been designed to be lightweight compared to the existing extended KF-based convergence system, but is more robust to both weak and hard NLOS environments. Eventually, it improved positioning performance by 35.5% than existing hybrid systems in the hard NLOS environments.

INDEX TERMS Indoor positioning, ultra-wideband (UWB), pedestrian dead-reckoning (PDR), Kalman filter (KF) sensor fusion, and hybrid positioning.

I. INTRODUCTION

With the proliferation of the Internet of Things (IoT), various location-based services (LBS) such as an indoor object search, entertainment, advertising, and marketing have been requested by users. Many users want LBS to be available in both indoor and outdoor environments. However, most LBSs are focused on outdoor services using a global navigation satellite system (GNSS), such as GPS and Galileo.

The indoor positioning system (IPS) was designed to provide LBS in an indoor environment where the GNSS cannot operate well owing to its weak signal. There are many approaches to building an IPS, such as time-based positioning methods [1]–[4], radio fingerprinting [5]–[7], and dead reckoning [8], [9]. Among these approaches, time-based positioning achieves an accurate and precise positioning performance. However, it requires a high-performance time-resolution medium such as ultra-wideband (UWB) radio, ultrasonic, and visible light. The extra requirements of this approach incur additional expenses. By contrast, fingerprint-based positioning can build a low-cost IPS using a universal medium such as WiFi, BLE, and cellular networks. However, it requires additional work, i.e., a fingerprint learning (offline) phase to construct the received signal strength (RSS) map, which is time-consuming and workload-intensive. Dead reckoning-based positioning can build a system without additional infrastructure, while using multimodal sensors such as accelerometers, gyroscopes, magnetometers, and barometers. However, it requires a reference position and needs to operate for a short run time because of accumulated errors over time [10]. Because of the trade-off between positioning methods, some existing positioning methods have been combined complementarily to provide a higher positioning performance [11]. In this study, we use both UWB and pedestrian dead reckoning (PDR) to produce robust continuous positioning in an indoor environment where each position is limited.

The UWB, defined in IEEE 802.15.4-2011 std. [12], supports an extremely accurate time-stamping and direct path selection capability based on impulse radio with nanoscale

The associate editor coordinating the review of this manuscript and approving it for publication was Mohamed Kheir.

time resolution. High-resolution time-stamping is used to accurately measure the propagation time in time-based ranging, and direct path selection is used to precisely classify the shortest signal path corresponding to the distance between UWB radios in a multipath environment. Owing to these advantages, UWB can be applied to time-based positioning, namely, time-of-arrival (TOA) and time-difference-of-arrival (TDOA) [1]–[4]. The TOA-based UWB positioning system determines the position of a tag device through trilateration by employing the known positions of pre-deployed anchors and the estimated distance between the tag and anchors. Here, the distance between the tag and anchors is obtained from a TOA estimation technique called two-way ranging (TWR) [12]. The TOA estimation through TWR can make the IPS easier to implement without device-to-device synchronization, compared to TDOA-based positioning systems [13]. Moreover, the UWB system has a fast position update rate with sub-meter-level positioning accuracy and precision [14]. However, the UWB system requires an infrastructure consisting of three or more anchors and a clear line-of-sight (LOS) channel between the tag and anchor without any obstacles. These requirements can be a limitation of UWB-based indoor LBS. However, positioning with an IMU consisting of an accelerometer, gyroscope, and magnetometer can estimate the attitude and heading using its measured values. Thus, it can be applied to dead reckoning of a flight and voyage. The PDR system based on the MEMS IMU is an infrastructure-free positioning method because it determines the position based on the step length of the pedestrian and its heading. Likewise, it is robust to external environmental factors such as the non-line-of-sight (NLOS) radio channel. However, the PDR requires an initial reference position because it is a relative positioning method in which the position is updated by adding displacement to the previous position. In addition, it is expected to be operating for a short run time because of drift error of distance and heading estimation accumulated as time passes.

These UWB and PDR systems can be fused to improve the positioning performance owing to their complementary characteristics. The UWB/PDR hybrid system mitigates the PDR drift based on the more accurate positioning results obtained from UWB and reduces the NLOS-caused error of the UWB with a stable output from the PDR. Valuable studies on UWB and PDR integration have been conducted. In [16], the authors proposed a PDR aided UWB positioning method to switch between two positioning systems. The position difference between the UWB and PDR is applied to its probability distribution-based formula. In [17], the weighted average was chosen as the fusion method. It mitigates the positioning error of the UWB through the PDR. As a more advanced approach, the authors of [18] proposed a new method using the position difference with an extended Kalman filter (EKF). These methods apply PDR as a substitute for UWB when UWB positioning is unavailable. However, these methods have difficulties determining whether the UWB channels are classified as LOS or NLOS. Meanwhile, the EKF fusion proposed in [19] recognizes abnormal UWB ranging based on the Mahalanobis distance approach and controls its noise covariance. It is effective for stabilizing the UWB ranging performance against temporary NLOS errors. However, outlier detection based on the Mahalanobis distance is limited in environments where the NLOS effect persists for a specific time owing to walls and obstacles. In addition, the unscented KF (UKF) based integration method has been introduced to improve the linearization problem of the EKF for indoor localization [20]. In [21], the residual-based NLOS identification and Sage-Husa adaptive filtering based UKF algorithm (ISR-UKF) are introduced. The ISR-UKF reduced the positioning error by approximately 75% compared to the UWB single positioning. In [22], another study shows the application of EKF and UKF to the positioning environments with multiple anchors to improve the accuracy and reduce the complexity of the deployment.

This paper proposes an efficient hybrid positioning system that is simpler than the EKF approach and more robust against weak NLOS environments such as a through-the-wall environment. The remainder of this paper is organized as follows. We describe the relevant techniques for UWB and PDR in Section II. Sections III and IV present the proposed fusion algorithm and the experimental results. Finally, we conclude the paper in Section V.

II. BACKGROUND

A. TWO-WAY RANGING (TWR)

The TWR is a message-exchange procedure for estimating the distance between UWB radios. It has the advantage of observing the estimated distance on both tag and anchor sides due to the message exchange. In this paper, the UWB system uses TWR performing TOA estimation because the tag has to obtain a position itself for integration with the PDR system. Fig. 1 shows the TWR introduced in IEEE 802.15.8 std. and IEEE 802.15.4-2011 std. [12], [15]. In Fig. 1, a tag device and an anchor are illustrated as T and A, respectively. First, the tag sends a ranging request message to the anchor and stores T_1 at the tag device as a TX timestamp. The anchor receives a request message from the tag and stores T_2 as an RX timestamp. Next, the anchor sends a response message to the tag after a reply time (T_{reply}) and stores T_3 at the anchor device as a TX timestamp. Finally, the tag stores T_4 after obtaining the response message as an RX timestamp.

In this typical TWR, timestamps are obtained by capturing the ranging marker designated in the UWB system. The ranging marker specified in [12] is located at the start of the first symbol of the PHY header of the frame. The round trip time (RTT) of the ranging messages is measured using timestamps (T_1, T_2, T_3, and T_4) observed in the tag and anchor as follows:

$$T_{round} = T_4 - T_1, \tag{1}$$

$$T_{reply} = T_3 - T_2, \tag{2}$$

$$T_{RTT} = T_{round} - T_{reply}. \tag{3}$$

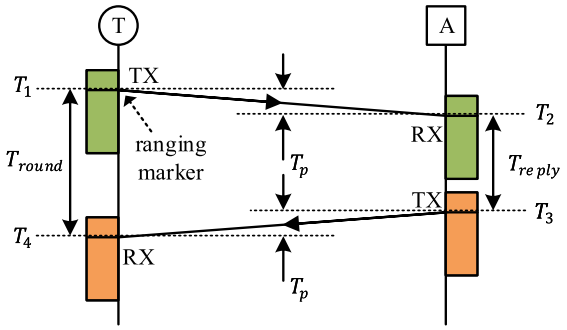

FIGURE 1. Two-way ranging (TWR).

In addition, the propagation time (T_p), that is, TOA of the ranging message, can be estimated as follows:

$$T_p = \frac{T_{RTT}}{2}. \tag{4}$$

Therefore, the distance between the tag and anchor is $d = T_p \times c$, where c is the speed of light.

As shown in Fig. 1, the TWR based TOA estimation does not demand time synchronization between tag and anchor because T_{round} and T_{reply} are observed independently at each device. This advantage makes it easier to build positioning systems. However, TWR based on single-sided RTT has a weakness in that the TOA estimation error can be increased by the longer TWR message processing time (T_{reply}) because of the hardware clock skew between the tag and anchor. Thus, the double-sided TWR (DS-TWR) was devised to solve the clock skew problem by measuring the RTT at each side of the tag and anchor. The DS-TWR procedure is illustrated in Fig. 2.

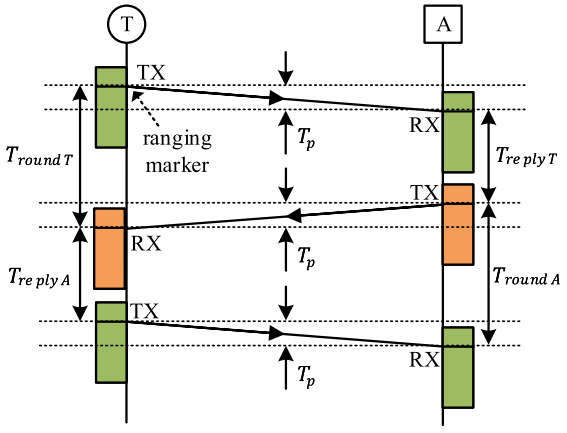

FIGURE 2. Double-sided TWR (DS-TWR).

In DS-TWR, the tag and anchor initiate a TWR message exchange, which is the same as typical TWR obtaining RTT on the tag side. After obtaining the first RTT, the tag sends a second ranging message to the anchor for the second RTT. Finally, the response of the anchor and second ranging messages of the tag are used to obtain the second RTT on the anchor-side during this process. Thus, T_p of the DS-TWR is measured by

$$T_p = \frac{T_{roundT} \times T_{roundA} - T_{replyT} \times T_{replyA}}{T_{roundT} + T_{roundA} + T_{replyT} + T_{replyA}}. \tag{5}$$

In general, the TWR-based UWB positioning system inevitably requires three or more anchors for the estimation of the tag location. Indeed, to provide the navigation services based on DS-TWR, each tag needs at least nine transfers because DS-TWR performs three message exchanges with three anchors. This operation requires a large on-air time and battery power to obtain the position of each tag. One of the commercial UWB manufacturers introduced a practical DS-TWR for its real-time location system (RTLS) service [23], which improved the power consumption and on-air time in TWR message exchanges.

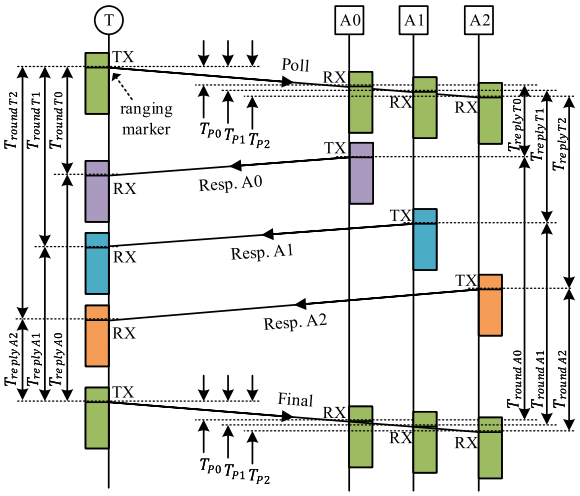

FIGURE 3. Decawave TWR (DW-TWR).

Fig. 3 shows the RTT measurement operation of the DW-TWR procedure. In this example, the tag initiates the broadcasting of a poll message to anchors (A0 $\sim$ A2). The anchors receiving a poll message from the tag then send response messages sequentially after a predefined reply time ($T_{replyT0}$, $T_{replyT1}$, and $T_{replyT2}$). Next, the tag receiving response messages from the anchors sends a final message to the anchors. Finally, the anchor receiving the final message completes the ranging message exchange. As a result, the propagation time T_{pN} for anchor number N is calculated by the stored timestamps as follows:

$$T_{pN} = \frac{T_{roundTN} \times T_{roundAN} - T_{replyTN} \times T_{replyAN}}{T_{roundTN} + T_{roundAN} + T_{replyTN} + T_{replyAN}}, \tag{6}$$

where N is 0, 1, and 2 in the example shown in Fig. 3.

B. NLOS IDENTIFICATION

The TOA estimation of the TWR is achieved using the propagation time (T_p) in the direct path, which is the closest distance between the tag and anchor. However, during the NLOS condition, the multipath propagation delay time is added to

the TOA estimation owing to the direct path weakening or disappearance. An NLOS identification method is required to mitigate positioning errors caused by the NLOS. In general, IR-UWB technology is more advantageous than narrowband communication for distinguishing the direct path and multipath signals and is analyzed as the channel impulse response (CIR). The CIR is the basis for classifying the channel conditions as an LOS or NLOS [2]. According to [23], the UWB receiver can measure the received signal strength of the direct path (*FSL*) and multipath (*RSL*) based on the observed CIR of the preamble code in the PHY layer. The difference (*GAP*) between *FSL* and *RSL* is small in the LOS channel. On the other hand, *GAP* is increased by attenuated *FSL* due to obstacles in the NLOS channel. Therefore, channel conditions can be classified as NLOS or LOS using *GAP* [24]. In [25], we proposed a new NLOS identification method applicable to various NLOS environments, including through-the-wall and curved corridor environments. Algorithm 1 denotes the proposed identification method. We applied this identification method to our proposed UWB/PDR hybrid positioning system to mitigate the NLOS error.

Algorithm 1 NLOS Identification for the Proposed Hybrid System

Input: FSL, RSL
Output: channel identification
Initialization: average RSL ($ARSL$) $= -87.1$ [dBm]
$GAP = RSL - FSL$; //gap between RSL and FSL
if $GAP > 10$ **then**
  return NLOS
else
  if $ARSL < RSL$ **then**
    return LOS
  else
    return NLOS

C. TRILATERATION

Trilateration is the process of determining an unknown position with a mathematical calculation for estimating the relative position by applying a geometry of circles and spheres. Fig. 4 shows anchors A0 $\sim$ A2 located in their known positions $(x_0, y_0) \sim (x_2, y_2)$, whereas the distances d0 $\sim$ d2 between a tag and anchors are obtained using the TWR. Here, the position of the tag (x, y) located at the intersection between the circles is obtained by the following:

$$\begin{cases} (x_0 - x)^2 + (y_0 - y)^2 = {d_0}^2, \\ (x_1 - x)^2 + (y_1 - y)^2 = {d_1}^2, \\ \qquad\qquad \vdots \\ (x_n - x)^2 + (y_n - y)^2 = {d_n}^2. \end{cases} \tag{7}$$

However, it is challenging to determine the real tag location with distances $(d_0, d_1, \ldots, d_n)$ in an erroneous positioning environment, because the positioning errors are added by the UWB signal strength fluctuation.

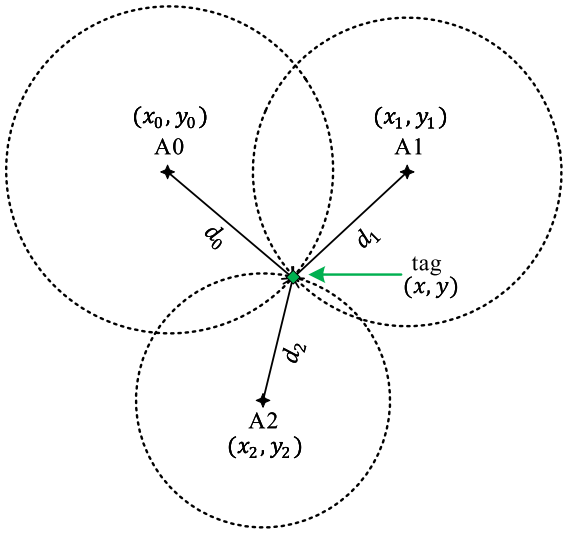

FIGURE 4. 2D localization using trilateration.

For practical positioning, we applied the well-known least squares (LS) method to solve (7). The LS method produces an approximation of the exact intersection of three circles by applying the form of a linear equation of $a\xi = b$ as follows:

$$a = \begin{bmatrix} x_1 - x_0 & y_1 - y_0 \\ x_2 - x_0 & y_2 - y_0 \\ \vdots & \vdots \\ x_n - x_0 & y_n - y_0 \end{bmatrix}, \tag{8}$$

$$\xi = \begin{bmatrix} x \\ y \end{bmatrix}, \tag{9}$$

$$b = \frac{1}{2} \begin{bmatrix} {x_1}^2 + {y_1}^2 - {d_1}^2 - ({x_0}^2 + {y_0}^2 - {d_0}^2) \\ {x_2}^2 + {y_2}^2 - {d_2}^2 - ({x_0}^2 + {y_0}^2 - {d_0}^2) \\ \vdots \\ {x_n}^2 + {y_n}^2 - {d_n}^2 - ({x_0}^2 + {y_0}^2 - {d_0}^2) \end{bmatrix}, \tag{10}$$

Now, the tag location is estimated as

$$\xi = (a^T a)^{-1} a^T b. \tag{11}$$

D. PEDESTRIAN DEAD RECKONING (PDR)

The PDR is a relative positioning method that estimates a new position based on pedestrian movement. The pedestrian step should be detected at every step, and measurements of the step length (SL) and heading are also required. Fig. 5 shows the PDR process for estimating a pedestrian's position. In Fig. 5, the pedestrian is walking from the initial position (red triangle) to the current position (blue circle). A movement trajectory consisting of SL and a heading is shown.

The current position is estimated as follows:

$$\begin{cases} x_n = x_{n-1} + SL \cdot -\cos(\psi), \\ y_n = y_{n-1} + SL \cdot \sin(\psi), \end{cases} \tag{12}$$

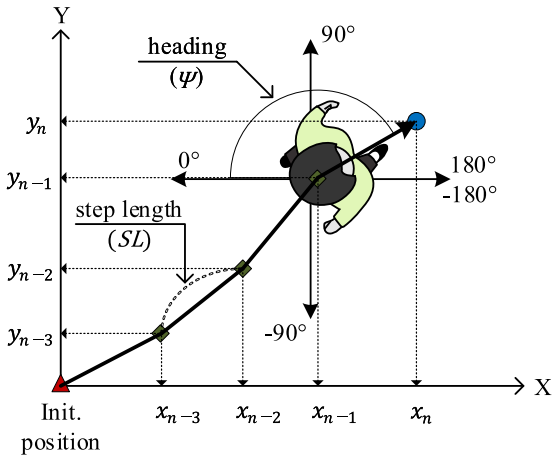

FIGURE 5. Pedestrian dead reckoning.

where n is the step count, beginning from the initial position, and SL and ψ are the step length and heading when a step is detected, respectively.

In the first stage, the pedestrian walking is detected by a step detection algorithm using acceleration obtained from a waist-mounted IMU device. We used the peak detection algorithm to count the peak of the acceleration while walking [20], [26]. This has an advantage in that it can be easily applied to the building of a PDR. Second, an acceleration-based SL estimation, also known as the Weinberg method, is performed [27].

The SL is estimated through the acceleration created by the waist bounce as follows:

$$SL = K \times \sqrt[4]{A_{max} - A_{min}}, \tag{13}$$

where K is a constant for a unit conversion, such as the feet or meters traveled. In addition, A_{max} and A_{min} are the maximum and minimum accelerations measured in a single stride, respectively.

The attitude heading reference system (AHRS) is a method applying a built-in accelerometer, gyroscope, and magnetometer in the IMU to calculate the attitude and heading expressed in Euler angles (ϕ, θ, ψ) [28]. The heading described by the Euler angle yaw (ψ) is obtained from AHRS as follows:

$$M_X = m_x \cos(\theta) + m_y \sin(\theta)\sin(\phi) + m_z \sin(\theta)\cos(\phi), \tag{14}$$

$$M_Y = m_y \cos(\phi) - m_z \sin(\phi), \tag{15}$$

$$\psi = \arctan(\frac{M_Y}{M_X}), \tag{16}$$

where m_x, m_y, and m_z are 3-axis magnetic field data from the magnetometer. In addition, ϕ and θ are the roll and pitch angles obtained from the accelerometer and gyroscope, respectively.

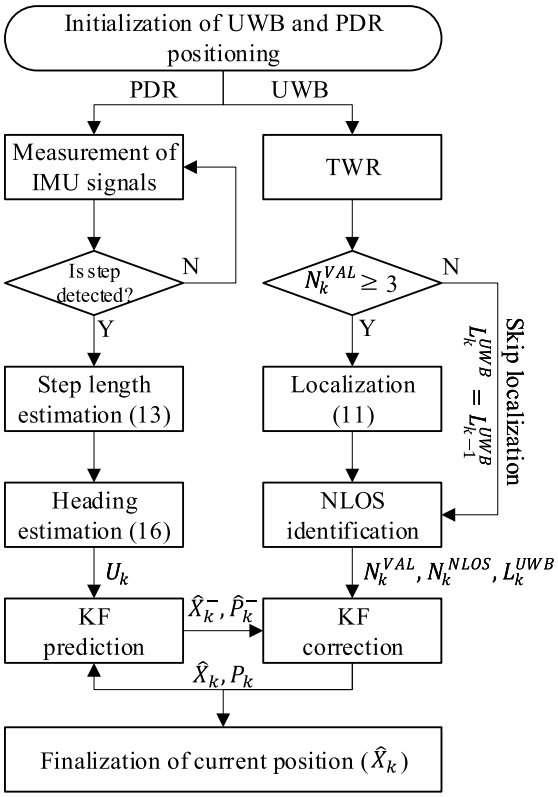

FIGURE 6. Proposed NLOS identification based UWB/PDR hybrid system (NI-hybrid system).

III. PROPOSED NLOS IDENTIFICATION BASED UWB/PDR HYBRID SYSTEM

The proposed positioning system integrates both UWB and PDR based on the KF sensor fusion method [29]. The KF can provide estimates of tag positions, given the measurements including noise observed over time. The KF consists of two phases: prediction and correction. In the prediction phase, the expected measurements for the system input are calculated, and in the correction phase, the current position is estimated from the predicted and actual measurements. In this paper, to estimate the tag positions even in an NLOS environment, the proposed method applies the NLOS identification algorithm to the measurement update stage of the KF. Fig. 6 shows the operation procedure of the proposed NLOS identification based UWB/PDR hybrid system (NI-hybrid system). In Fig. 6, the PDR and UWB systems are linked to the prediction and correction phases of the KF. When the PDR system detects a new step k, the step length estimation algorithm observes the step length (SL_k) for k by applying (13). Next, the heading estimation process finds the heading (ψ_k) for k with (16). Finally, the SL_k and ψ_k obtained are input into the KF prediction, also known as the time update phase. Concurrently, the UWB system performs TWR and then finds the tag location using trilateration. During this process, the UWB system needs to count the number of valid TWRs (N_k^{VAL}), which can estimate the distance between

the tag and each anchor. If N_k^{VAL} is greater than or equal to three, the UWB system updates the UWB position (L_k^{UWB}) from a previous UWB position (L_{k-1}^{UWB}) with the LS estimation (9). Subsequently, the NLOS identification process calculates the number of valid TWRs in the NLOS channel (N_k^{NLOS}). Finally, the L_k^{UWB}, N_k^{VAL}, and N_k^{NLOS} obtained are input into the KF correction, also known as the measurement update phase. The proposed system follows the principle of the discrete KF [29], such that the position is updated at each step of the pedestrian. By operating both the prediction and correction phases recursively, the proposed system provides a combined positioning result.

For the KF prediction phase, we set the state equation for the 2D current position ($X_k = \begin{bmatrix} x_k & y_k \end{bmatrix}^T$) of the new step k as follows:

$$X_k = AX_{k-1} + BU_k + w_k, \tag{17}$$

where A and B are the set identity matrices, and w_k is the process noise. In addition, U_k is the system input vector, which denotes the movement of the pedestrian at step k.

$$U_k = \begin{bmatrix} SL_k \cdot -\cos(\psi_k) \\ SL_k \cdot \sin(\psi_k) \end{bmatrix}, \tag{18}$$

For the correction phase, we set up the measurement process using the UWB system as follows:

$$Z_k = L_k^{UWB} = HX_k + v_k, \tag{19}$$

where $L_k^{UWB} = \begin{bmatrix} ux_k & uy_k \end{bmatrix}^T$ is the updated position of the UWB system, H is set to the identity matrix, and v_k denotes the measurement noise.

In this study, the process noise covariance $Q = diag(\sigma_{px}^2, \sigma_{py}^2)$ of the PDR system model is considered fixed because it is less affected by external factors such as radio channel conditions. By contrast, the measurement noise covariance $R = diag(\sigma_{ux}^2, \sigma_{uy}^2)$, which is the error covariance of the UWB system, is variable because of the NLOS effect.

We assume that the tag and anchor exposed to the NLOS will have a nonstationary UWB signal. In this NLOS environment, if $N_k^{VAL} < 3$, the covariance matrix R will be large. However, when all anchors are in the LOS condition, R will be smaller. Therefore, the updated R_k can be expressed as depending on the weight factor W_k as follows:

$$W_k = \begin{cases} \frac{N_k^{NLOS}}{N_k^{VAL}}, & \text{if } N_k^{VAL} \geq 3 \\ 1, & \text{if } N_k^{VAL} < 3 \end{cases} \tag{20}$$

$$R_k = R_{min} \cdot \left(\frac{R_{max}}{R_{min}}\right)^{W_k} \quad \text{for } 0 \leq W_k \leq 1, \tag{21}$$

where R_{min} and R_{max} are the minimum and maximum the values of R, respectively, N_k^{VAL} is the number of valid TWRs, and N_k^{NLOS} is the number of anchors in the NLOS channel. In addition, if $N_k^{VAL} < 3$, W_k is set to 1, regardless of N_k^{NLOS}. Algorithm 2 describes the procedure for the NLOS identification KF (NI-KF) fusion.

Algorithm 2 NLOS Identification KF (NI-KF) Fusion

Input: $SL_k, \psi_k, N_k^{VAL}, N_k^{NLOS}, L_k^{UWB}$
Output: $\hat{X}_k$
Initialization: $R_0 = Rmin, \hat{X}_0 = L_k^{UWB}$
for $k = 0 : n$ **do**

Func `Prediction` $(SL_k, \psi_k, \hat{X}_{k-1}, P_{k-1})$ **:**

$$U_k = \begin{bmatrix} SL_k \cdot -\cos(\psi_k) & SL_k \cdot \sin(\psi_k) \end{bmatrix}^T$$

$$\hat{X}_k^- = A\hat{X}_{k-1} + BU_k$$
$$P_k^- = AP_{k-1}A^T + Q$$

return $\hat{X}_k^-, P_k^-$

Func `Correction` $(N_k^{VAL}, N_k^{NLOS}, L_k^{UWB}, \hat{X}_k^-, P_k^-)$ **:**

if $N_k^{VAL} \geq 3$ **then**
$W_k = \frac{N_k^{NLOS}}{N_k^{VAL}}$
else
$W_k = 1$

$$R_k = R_{min} \cdot \left(\frac{R_{max}}{R_{min}}\right)^{W_k}$$
$$Z_k = L_k^{UWB}$$

$$K_k = P_k^- H^T (HP_k^- H^T + R_k)^{-1}$$
$$\hat{X}_k = \hat{X}_k^- + K_k(Z_k - H\hat{X}_k^-)$$
$$P_k = P_k^- - K_k HP_k^-$$

return $\hat{X}_k, P_k$

IV. PERFORMANCE EVALUATION

A. EXPERIMENTAL SETUP

In this section, we introduce our testbed for the performance evaluation of the proposed UWB/PDR positioning system. The testbed consists of a tag as the positioning target and anchors deployed in the experimental area. The tag device we developed in this study has functions of the UWB and PDR positioning and consists of five parts, as shown in Fig. 7. The parts of the tag device are (A) UWB module (DWM1000), (B) IMU module (EBIMU-9DOF), (C) Bluetooth module (FB155BC), and (D) and (E) microcontroller units (MCU) (STM32F105 and STM32F407, respectively). In our tag device, the sub-controller (D) controls (A) to perform the TWR and report the results of the TWR to the main controller (E). Next, (E) drives the NI-KF fusion algorithm with the UWB system of (D) and the PDR system (B). The user can access internal data through (C). The anchors used in this study are EVB1000 devices developed by Decawave, and include only the UWB system, such as (A) and (D), of the

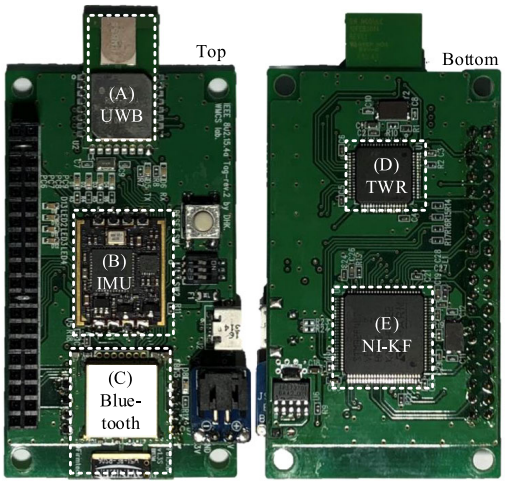

FIGURE 7. The tag device of the UWB/PDR hybrid system.

tag device. In this evaluation, we configured the parameters of each system as follows:

1) PDR SYSTEM

The accelerometer has a sensitivity of 16 g, a gyroscope has a sensitivity of 2000°s, the sensitivity of the magnetometer is 0.6 uT, the sampling frequency is 50 Hz, a step length factor K of 0.75 is applied, and the heading offset from the earth frame is 20°.

2) UWB SYSTEM

A total of three channels are used, the pulse repetition frequency (PRF) is 16 MHz, the data rate is 110 Kbps, the preamble length is 1024, the preamble code is 5, and a TWR duration of 280 ms is applied.

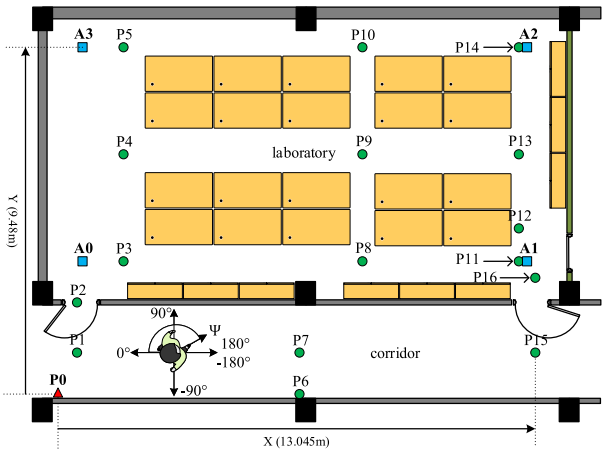

FIGURE 8. The experiment area with reference points and azimuth.

The experimental area chosen for testing was a general indoor NLOS environment. Fig. 8 shows the experimental area consisting of a laboratory, corridor, and furniture, as well as the deployment of UWB anchors. In this figure, there

TABLE 1. Coordinates (x, y) [m] of the reference points.

Ref.	Coordinates (x, y) [m]	Ref.	Coordinates (x, y) [m]	Ref.	Coordinates (x, y) [m]
A0	(0.67, 3.62)	A1	(12.82, 3.62)	A2	(12.82, 9.47)
A3	(0.67, 9.47)	P0	(0, 0)	P1	(0.52, 1.125)
P2	(0.52, 2.4)	P3	(1.79, 3.62)	P4	(1.79, 6.545)
P5	(1.79, 9.47)	P6	(6.6, 0)	P7	(6.6, 1.125)
P8	(8.32, 3.62)	P9	(8.32, 6.545)	P10	(8.32, 9.47)
P11	(12.6, 3.62)	P12	(12.6, 4.52)	P13	(12.6, 6.545)
P14	(12.6, 9.47)	P15	(13.045, 1.125)	P16	(13.045, 3.17)

are three types of reference points. The red triangle P0 is the origin of a 2D coordinate system, the blue rectangles A0 ∼ A3 are pre-installed UWB anchors, and the green circles P1 ∼ P16 are waypoints on the path of a moving target. Table 1 lists the coordinates of these reference points. The tag is held at the user's chest height of 1.4 m, and the anchors are deployed at the height of 1.8 m. The relative height difference of 0.4 m between the tag and anchor is ignored in this evaluation because it does not almost affect the 2D LS-based positioning performance [30]. In addition, to match the azimuth angle with the 2D coordinate system, a bias with a heading offset of 20° is added when obtaining the heading yaw.

Fig. 9 shows the overall experimental environment with pre-deployed anchors. Each sub-figure was taken on specific waypoints in the experiment area. Fig. 9 (a) shows area P4, whereas Fig. 9 (b) shows area P13 in the laboratory and corridor.

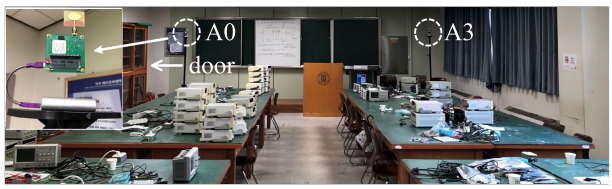

(a)

(b)

FIGURE 9. The experiment area and anchor deployment: (a) laboratory (A0 and A3) and (b) laboratory (A1 and A2), and corridor.

B. EXPERIMENTAL SCENARIOS

In this experiment, we considered two scenarios. The first scenario is in a weak NLOS environment caused by obstacles such as furniture or the human body, which are frequently observed in various situations and result in a relatively small error. The second scenario is in a hard NLOS area, such as

with concrete walls and compartments. In general, when the tag moves to the hard NLOS area where UWB anchors are not installed, the positioning performance is more severe. The experimental area shown in Fig. 8, is divided into a laboratory and corridor by walls and furniture. The UWB anchors were placed only in the laboratory. In other words, the weak NLOS scenario was built in the laboratory, whereas the hard NLOS scenario was formed in the corridor.

In addition, we created different paths for each scenario and compared our proposed positioning with existing positioning techniques. In each path, the mobile tag departs from the first waypoint, passes through the next waypoints one by one directly, and then arrives at the last waypoint. Table 2 lists the waypoints for each path used in the scenario. Existing positioning methods can be divided into two types. The first is the non-fusion method such as UWB and PDR. The second is a fusion method using KF or EKF. For the KF-based fusion methods, a typical KF and proposed NI-KF could be used. The operations of the prediction and correction phases in hybrid-1 using typical KF are the same as the proposed one using NI-KF. However, there is no method to update the measurement noise covariance in KF fusion based on NLOS identification. The EKF-based fusion presented in [18] and [19] are labeled hybrid-2 and hybrid-3, respectively.

TABLE 2. Waypoints of each trajectory used in the scenario.

Environments	Scenarios	Waypoints
Weak NLOS	Square 1	P4, P9, P8, P3, P4
Weak NLOS	Square 2	P4, P13, P11, P3, P4
Weak NLOS	Zigzag	P3, P5, P10, P8, P11, P14
Hard NLOS	Clockwise 1	P4, P13, P11, P16, P15, P1, P2, P3, P4
Hard NLOS	Clockwise 2	P4, P9, P8, P11, P16, P15, P6, P1, P2, P3, P4
Hard NLOS	Counterclockwise	P4, P3, P2, P1, P15, P16, P11, P8, P9, P4

C. PERFORMANCE EVALUATION

For the positioning performance evaluation, we show a 2D trajectory, cumulative distribution function (CDF), box plot, and root mean square error (RMSE). The CDF, box plot, and RMSE were drawn based on the positioning error for each method. On each blue box in the box plot, the central red line indicates the median of the positioning error, and the bottom and top edges of the box indicate errors of 25% and 75%, respectively. The whiskers outside the box extend to the maximum and minimum error points not considered outliers, and the outliers are plotted individually using the red plus symbol.

The parameters of the hybrid-2 and hybrid-3 are the same as in [18] and [19], and NI-hybrid is configured as follows: Q and R_{min} are the identity matrices, and R_{max} is $diag(10^3, 10^3)$. In addition, the hybrid-1 uses Q and R of the identity matrix.

1) WEAK NLOS ENVIRONMENT

Figs. 10, 11, 12, and Table 3 indicate positioning performances for each method under the weak NLOS environment.

TABLE 3. RMSE [m] for positioning methods in weak NLOS environment.

Methods	Square 1	Square 2	Zigzag
UWB	0.3264	0.5031	0.6012
PDR	0.3154	0.721	0.7441
Hybrid-1	0.2625	0.4188	0.5690
Hybrid-2	0.294	0.4407	0.5886
Hybrid-3	0.2508	0.3751	0.54
NI-hybrid	0.2337	0.3895	0.5559

In the first square 1 scenario, the fusion-algorithm-based positioning systems (hybrid-1, hybrid-2, hybrid-3, and NI-hybrid) achieved a similar performance with an accuracy of approximately 0.25 m in terms of positioning error, and the positioning performance showed improvement compared to single positioning technology (UWB and PDR). Among these algorithms, the UWB approach without any sensor fusions has the lowest performance with a wide distribution of errors. By contrast, NI-hybrid has no outliers and the smallest RMSE. The next scenarios are square 2 and a zigzag showing an extended path from square 1. Along these longer paths, the accumulated PDR errors are observed, and UWB positioning has an outlier owing to the weak NLOS along their trajectories. By contrast, all fusion-based positioning methods effectively mitigate the drawbacks of UWB and PDR. In particular, NI-hybrid and hybrid-3 have a better accuracy and precision compared to hybrid-1 and hybrid-2.

As a result, the proposed NI-hybrid system has a similar performance to the existing EKF-based fusion system in a weak NLOS environment. Nevertheless, NI-KF is advantageous for systems with less computing power because most of the system matrices are determined as identity matrices, and the matrix dimension is small. In addition, it does not undergo a linearization step such as with a Jacobian approach.

2) HARD NLOS ENVIRONMENT

Figs. 13, 14, 15, and table 4 indicate positioning performances for each method under the hard NLOS conditions. Three scenarios, clockwise 1, clockwise 2, and counterclockwise, are used for this environment. In our testbed used for the hard NLOS conditions, all paths include a laboratory where anchors are placed and a corridor where they are not. Thus, note that the through-the-wall situation caused by the object penetration feature of UWB the curves at the halfway point of each path.

Along each trajectory, the PDR represents a similar drift error over all paths as a weak NLOS. However, the UWB shows worse positioning errors around the center of the corridor and door owing to the hard NLOS. By contrast, from coordinates of approximately (2, 1.5) to (4, 1.5) and from (10, 1.5) to (12, 1.5), a temporary recovery of the UWB channel is occasionally observed.

The hybrid-1 approach mitigates UWB outliers by using PDR positioning and improves the performance, although its measurement noise model does not correspond to the through-the-wall situation. As a result, unstable UWB signals

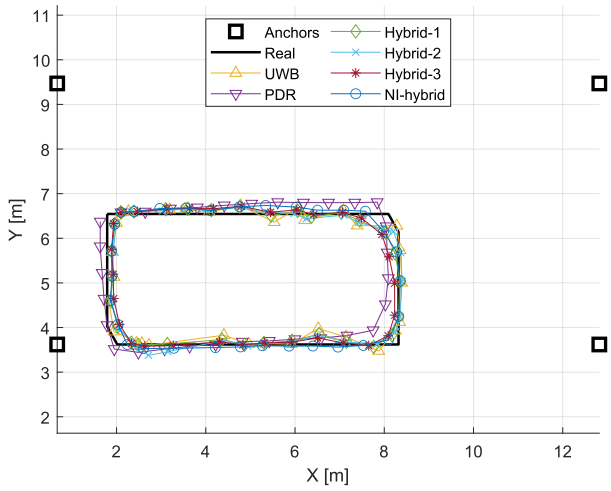

(a)

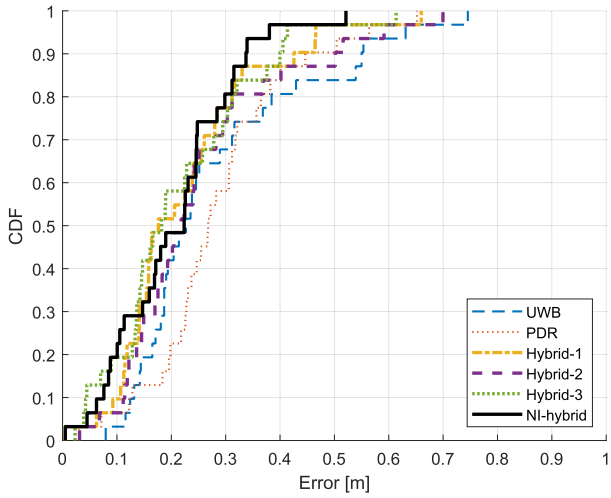

(b)

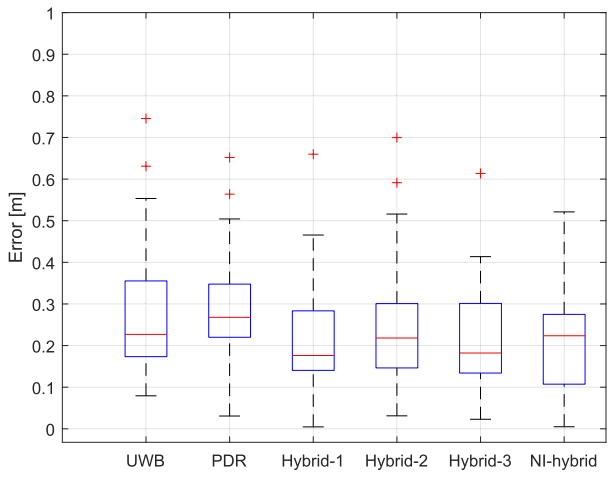

(c)

FIGURE 10. Positioning performances for each method in square 1 scenario: (a) positioning trajectories, (b) CDF of positioning error, (c) box plot of positioning error.

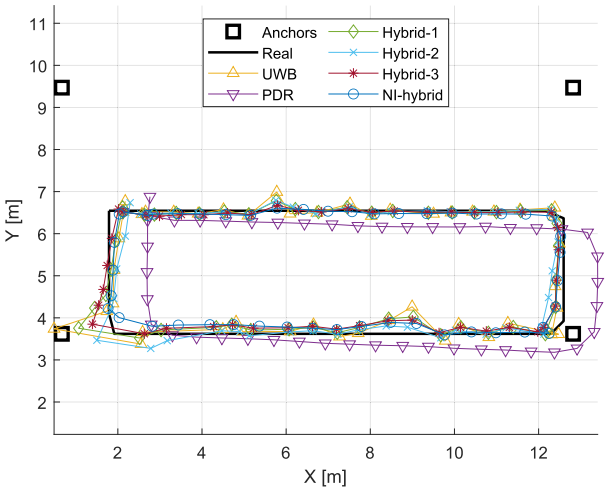

(a)

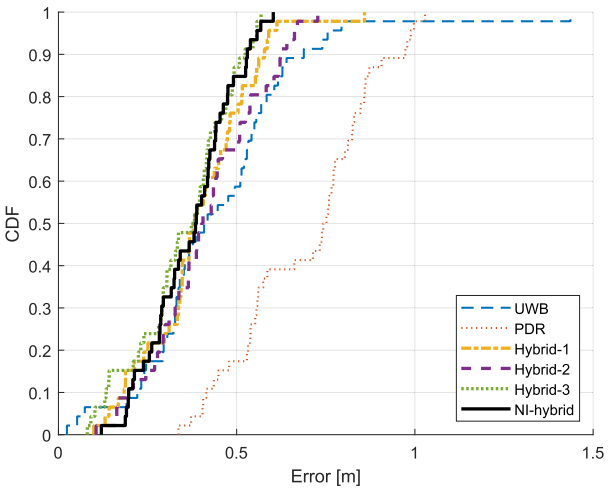

(b)

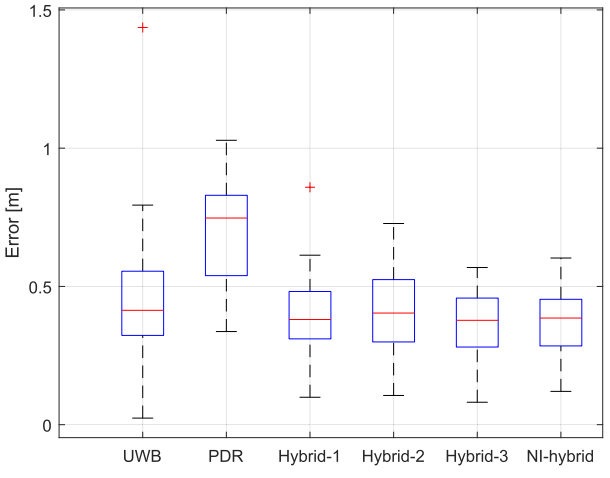

(c)

FIGURE 11. Positioning performances for each method in square 2 scenario: (a) positioning trajectories, (b) CDF of positioning error, and (c) box plot of positioning error.

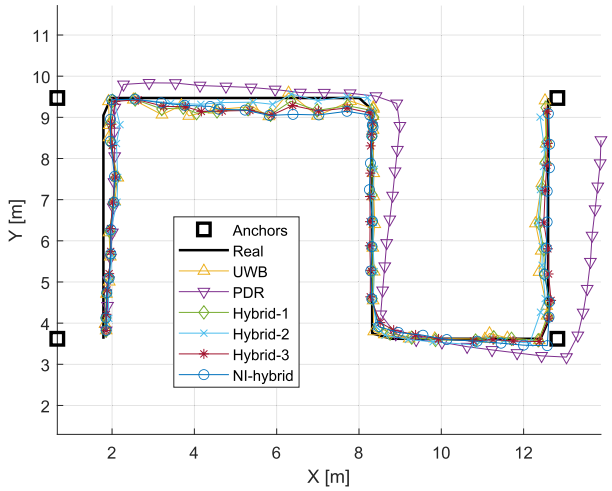

(a)

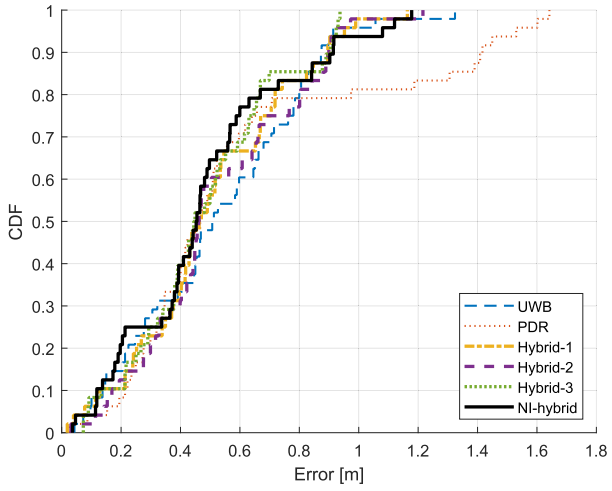

(b)

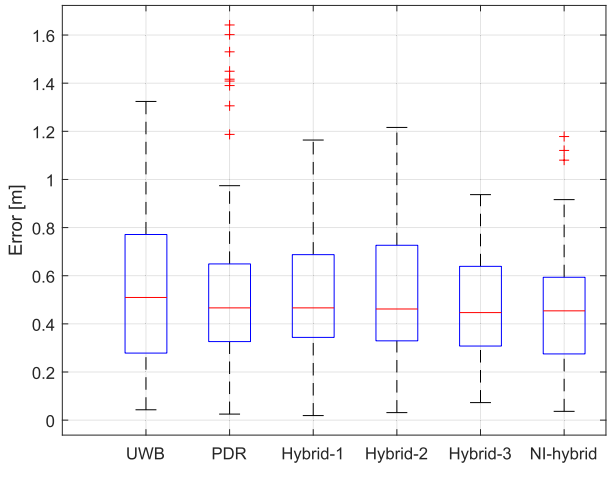

(c)

FIGURE 12. Positioning performances for each method in zigzag scenario: (a) positioning trajectories, (b) CDF of positioning error, and (c) box plot of positioning error.

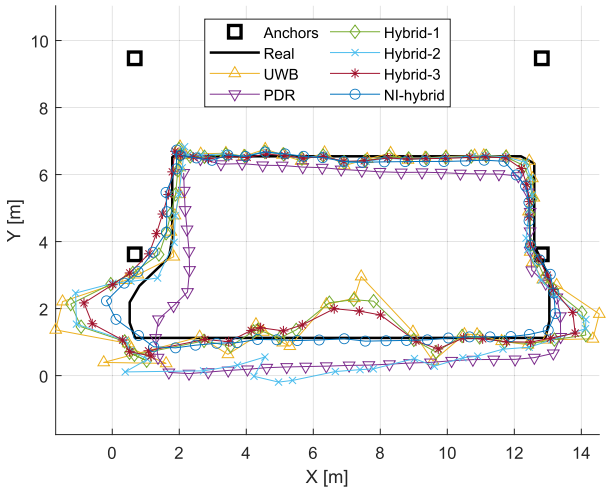

(a)

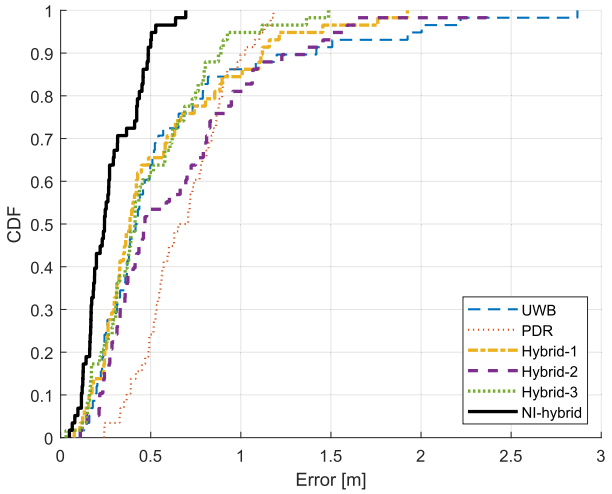

(b)

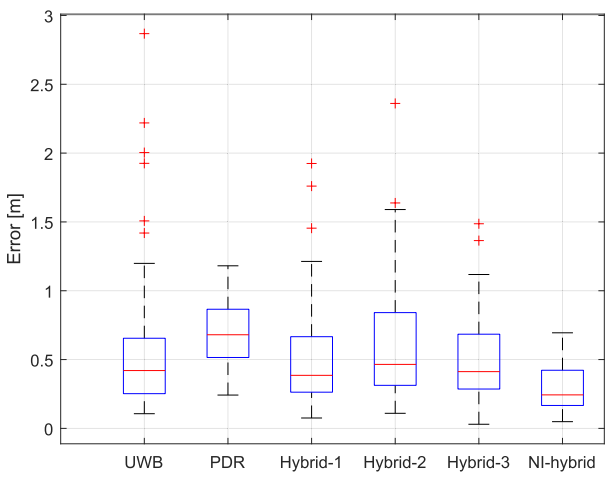

(c)

FIGURE 13. Positioning performances for each method in clockwise 1 scenario: (a) positioning trajectories, (b) CDF of positioning error, and (c) box plot of positioning error.

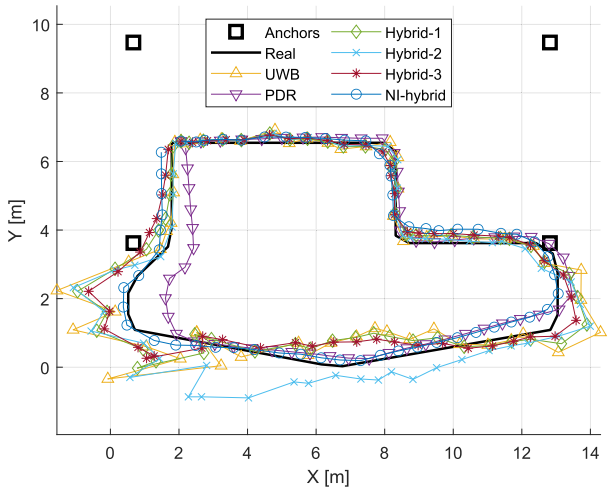

(a)

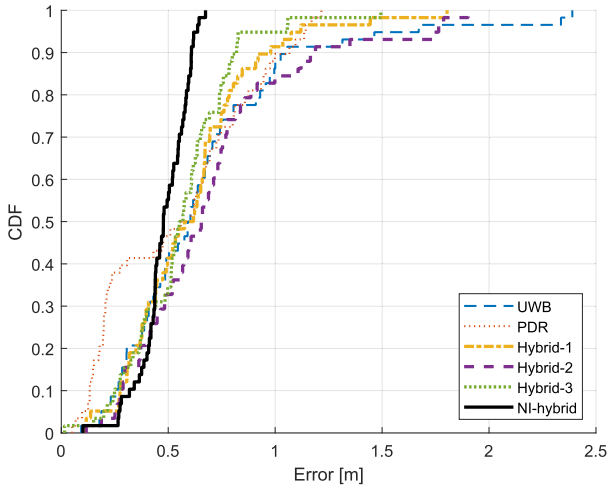

(b)

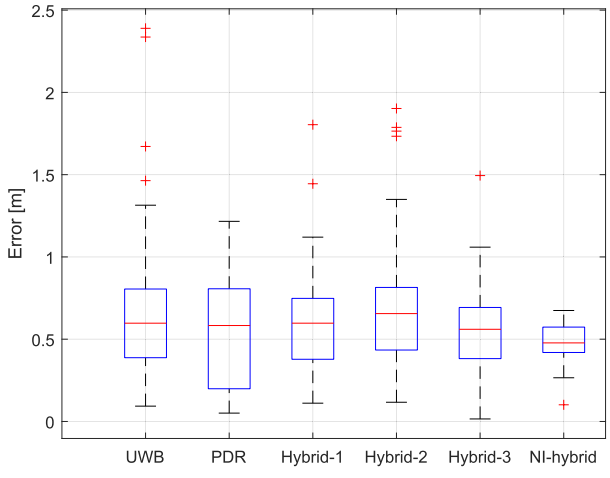

(c)

FIGURE 14. Positioning performances for each method in clockwise 2 scenario: (a) positioning trajectories, (b) CDF of positioning error, and (c) box plot of positioning error.

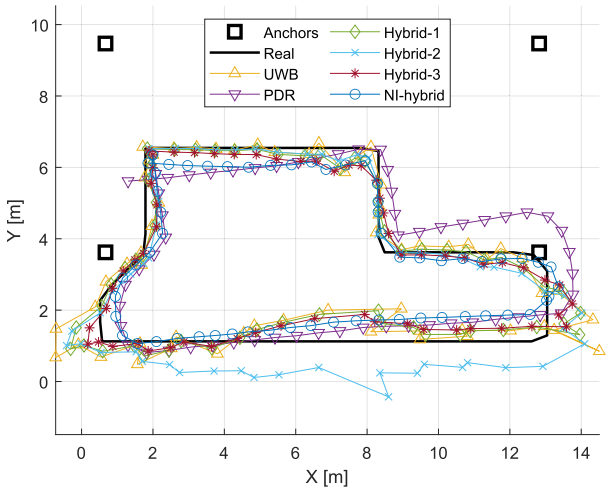

(a)

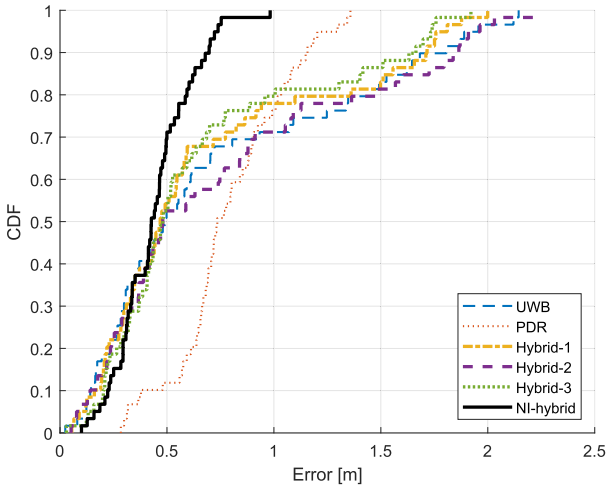

(b)

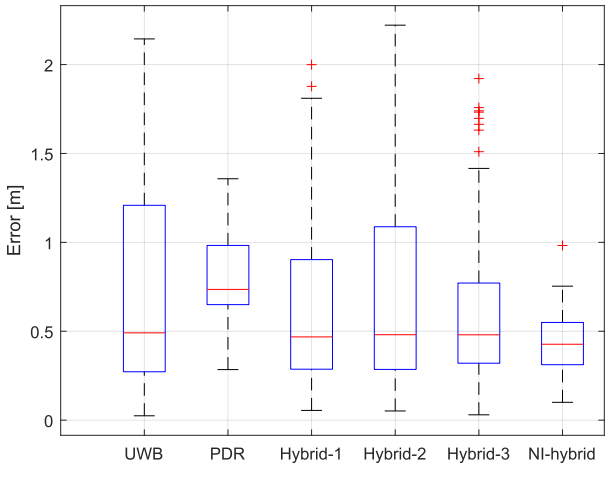

(c)

FIGURE 15. Positioning performances for each method in counterclockwise scenario: (a) positioning trajectories, (b) CDF of positioning error, and (c) box plot of positioning error.

TABLE 4. RMSE [m] for positioning methods in the hard NLOS environment.

Methods	Clockwise 1	Clockwise 2	Counterclockwise
UWB	0.8094	0.8071	0.9529
PDR	0.7254	0.6404	0.8339
Hybrid-1	0.6685	0.677	0.8791
Hybrid-2	0.7917	0.8083	0.9807
Hybrid-3	0.5744	0.6114	0.8302
NI-hybrid	0.3143	0.4923	0.4732

are observed along the trajectory. The hybrid-2 mitigates UWB errors at the beginning of the corridor, whereas some of them remained at each trajectory because of the persistent NLOS environments. It is clear that the hybrid-2 has a limitation in its application to hard NLOS environments owing to its reduced positioning performance. The hybrid-3 improves the positioning performance compared to hybrid-1 and hybrid-2 because it provides robustness under situations where UWB cannot update its position. However, outliers of the UWB were still observed in the trajectories. Under these scenarios, the TWR was successfully applied in the corridor, despite the anchor being installed behind the wall. That is, the UWB updates its position with higher errors observed in a hard NLOS channel. The observed error distribution under this scenario creates curves in the CDF and extends the whiskers in the box plot. The result of hybrid-3 shows the limitations of its system model, which is similar to the results of a KF without the NLOS identification approach.

NI-hybrid fuses PDR and UWB by evaluating the stability of the UWB through NLOS identification. In the corridor, the UWB fluctuations observed around each door and central area were alleviated by the PDR, and the drift of the PDR was calibrated using a temporary recovery of the UWB link. This calibration is observed from (2, 1.5) to (4, 1.5) and from (8, 1.5) to (10, 1.5) coordinates located in the corridor. Therefore, we conclude that NI-hybrid effectively mitigates the NLOS errors caused by the through-the-wall condition. This improvement is illustrated in the CDFs with enhanced slopes and box plots with the smallest boxes and shortest whiskers. Indeed, the average RMSE of the NI-hybrid is 0.4266 m, which is a 36.5% improvement in the positioning performance over 0.672 m for the hybrid-3.

V. CONCLUSION

In this paper, we proposed a UWB and PDR hybrid positioning system using an NLOS identification-based KF sensor fusion method. The proposed method was compared with existing hybrid methods in two experimental environments (weak NLOS and hard NLOS). In a weak NLOS environment, the proposed approach and the hybrid-3-based positioning systems show better performances than the others. Even in a hard NLOS environment, the proposed method shows an improvement in the RMSE of 36.5% compared to the existing system based on an EKF. The experimental results show that the proposed positioning system is robust to NLOS errors occurring at indoor environments. Moreover, our NI-hybrid system is lightweight compared to complex algorithms such as hybrid-2 and hybrid-3. It is clear that the NLOS environment has significantly degraded UWB positioning systems. We are considering using deep learning to enhance the NLOS identification performance of the proposed system in the future.

REFERENCES

[1] X. Cheng, A. Thaeler, G. Xue, and D. Chen, "TPS: A time-based positioning scheme for outdoor wireless sensor networks," in *Proc. IEEE INFOCOM*, vol. 4, Hong Kong, Mar. 2004, pp. 2685–2696.
[2] Z. Sahinoglu, S. Gezici, and I. Guvenc, *Ultra-Wideband Positioning Systems: Theoretical Limits Ranging Algorithms and Protocols*. Cambridge, U.K.: Cambridge Univ. Press, 2008.
[3] M. Hazas and A. Hopper, "Broadband ultrasonic location systems for improved indoor positioning," *IEEE Trans. Mobile Comput.*, vol. 5, no. 5, pp. 536–547, May 2006.
[4] T.-H. Do and M. Yoo, "An in-depth survey of visible light communication based positioning systems," *Sensors*, vol. 16, no. 5, p. 678, May 2016.
[5] H. Li, L. Sun, H. Zhu, X. Lu, and X. Cheng, "Achieving privacy preservation in WiFi fingerprint-based localization," in *Proc. IEEE Conf. Comput. Commun. (INFOCOM)*, Toronto, ON, Canada, Apr. 2014, pp. 2337–2345.
[6] B. Molina, E. Olivares, C. E. Palau, and M. Esteve, "A multimodal fingerprint-based indoor positioning system for airports," *IEEE Access*, vol. 6, pp. 10092–10106, Jan. 2018.
[7] C. Takenga and K. Kyamakya, "A low-cost fingerprint positioning system in cellular networks," in *Proc. 2nd Int. Conf. Commun. Netw. China*, Shanghai, China, Aug. 2007, pp. 915–920.
[8] A. R. Pratama, Widyawan, and R. Hidayat, "Smartphone-based pedestrian dead reckoning as an indoor positioning system," in *Proc. Int. Conf. Syst. Eng. Technol. (ICSET)*, Bandung, Indonesia, Sep. 2012, pp. 1–6. [Online]. Available: https://ieeexplore.ieee.org/abstract/document/6339316
[9] A. R. Jiménez, F. Seco, F. Zampella, J. C. Prieto, and J. Guevara, "Improved heuristic drift elimination (iHDE) for pedestrian navigation in complex buildings," in *Proc. Int. Conf. Indoor Positioning Indoor Navigat.*, Guimaraes, Portugal, Sep. 2011, pp. 1–8.
[10] R. K. Yadav, B. Bhattarai, H.-S. Gang, and J.-Y. Pyun, "Trusted *K* nearest Bayesian estimation for indoor positioning system," *IEEE Access*, vol. 7, pp. 51484–51498, Apr. 2019.
[11] S. Subedi, H.-S. Gang, N. Y. Ko, S.-S. Hwang, and J.-Y. Pyun, "Improving indoor fingerprinting positioning with affinity propagation clustering and weighted centroid fingerprint," *IEEE Access*, vol. 7, pp. 31738–31750, Mar. 2019.
[12] *IEEE Standard for Local and Metropolitan Area Networks—Part 15.4: Low-Rate Wireless Personal Area Networks (LR-WPANs)*, IEEE Standard 802.15.4-2011 (Revision of IEEE Standard 802.15.4-2006), 2011, pp. 1–314.
[13] J. Tiemann, Y. Elmasry, L. Koring, and C. Wietfeld, "ATLAS FaST: Fast and simple scheduled TDOA for reliable ultra-wideband localization," in *Proc. Int. Conf. Robot. Autom. (ICRA)*, Montreal, QC, Canada, May 2019, pp. 2554–2560.
[14] F. Hammer, R. Yudanto, K. Neumann, M. Pichler, J. Cockx, C. Niestroj, and F. Petre, "Performance evaluation of 3D-position estimation systems," *IEEE Sensors J.*, vol. 16, no. 16, pp. 6416–6424, Aug. 2016.
[15] *IEEE Standard for Wireless Medium Access Control (MAC) and Physical Layer (PHY) Specifications for Peer Aware Communications (PAC)*, IEEE Standard 802.15.8-2017, 2018, pp. 1–322.
[16] M. Xia, C. Xiu, D. Yang, and L. Wang, "A novel PDR aided UWB indoor positioning method," in *Proc. Ubiquitous Positioning, Indoor Navigat. Location-Based Services (UPINLBS)*, Wuhan, China, Mar. 2018, pp. 1–7.
[17] H. Tong, N. Xin, X. Su, T. Chen, and J. Wu, "A robust PDR/UWB integrated indoor localization approach for pedestrians in harsh environments," *Sensors*, vol. 20, no. 1, p. 193, Dec. 2019.
[18] F. Liu, J. Wang, J. Zhang, and H. Han, "An indoor localization method for pedestrians base on combined UWB/PDR/floor map," *Sensors*, vol. 19, no. 11, p. 2578, Jun. 2019.
[19] X. Li, Y. Wang, and K. Khoshelham, "UWB/PDR tightly coupled navigation with robust extended Kalman filter for NLOS environments," *Mobile Inf. Syst.*, vol. 2018, pp. 1–14, Dec. 2018.
[20] P. Chen, Y. Kuang, and X. Chen, "A UWB/improved PDR integration algorithm applied to dynamic indoor positioning for pedestrians," *Sensors*, vol. 17, no. 9, p. 2065, Sep. 2017.

[21] Y. Liu, S. Li, Q. Sun, C. Chang, G. He, and X. Kang, "An UWB/PDR fusion algorithm based on improved square root unscented Kalman filter," in *Proc. Chin. Control Conf. (CCC)*, Guangzhou, China, Jul. 2019, pp. 4124–4129.
[22] D. Feng, C. Wang, C. He, Y. Zhuang, and X.-G. Xia, "Kalman-filter-based integration of IMU and UWB for high-accuracy indoor positioning and navigation," *IEEE Internet Things J.*, vol. 7, no. 4, pp. 3133–3146, Apr. 2020.
[23] Decawave. (2017). *DW1000 User Manual*. [Online]. Available: https://www.decawave.com
[24] A. Albaidhani, A. Morell, and J. L. Vicario, "Ranging in UWB using commercial radio modules: Experimental validation and NLOS mitigation," in *Proc. Int. Conf. Indoor Positioning Indoor Navigat. (IPIN)*, Oct. 2016, pp. 1–7.
[25] D.-H. Kim, G.-R. Kwon, J.-Y. Pyun, and J.-W. Kim, "NLOS identification in UWB channel for indoor positioning," in *Proc. 15th IEEE Annu. Consum. Commun. Netw. Conf. (CCNC)*, Las Vegas, NV, USA, Jan. 2018, pp. 1–4.
[26] G. Palshikar, "Simple algorithms for peak detection in time-series," in *Proc. 1st Int. Conf. Adv. Data Anal., Bus. Anal. Intell.*, vol. 122, 2009, pp. 1–14.
[27] H. WeinBerg, "Using the ADXL202 in pedometer and personal navigation applications," Analog Devices, Norwood, MA, USA, Appl. Note AN-602, 2002, pp. 1–6.
[28] M. S. Islam, M. Shajid-Ul-Mahmud, T. Islam, M. S. Amin, and M. Hossam-E-Haider, "A low cost MEMS and complementary filter based attitude heading reference system (AHRS) for low speed aircraft," in *Proc. 3rd Int. Conf. Electr. Eng. Inf. Commun. Technol. (ICEEICT)*, Dhaka, Bangladesh, Sep. 2016, pp. 1–5.
[29] G. Welch and G. Bishop, "An introduction to the Kalman filter," Dept. Comput. Sci., Univ. North Carolina Chapel Hill, Chapel Hill, NC, USA, Tech. Rep. TR 95-041, 2006.
[30] A. Martinelli, M. Dolfi, S. Morosi, L. Mucchi, M. Paoli, and A. Agili, "Ultra-wide band positioning in sport: How the relative height between the transmitting and the receiving antenna affects the system performance," *Int. J. Wireless Inf. Netw.*, vol. 27, no. 1, pp. 18–29, Mar. 2020.

DAE-HO KIM received the B.S. and M.S. degrees in information and communication engineering from Chosun University, South Korea, in 2015 and 2017, respectively, where he is currently pursuing the Ph.D. degree. He is also a Researcher with the Wireless and Mobile Communication System Laboratory. His research interests include communication protocols and network systems for IoT services, indoor positioning systems (IPSs), and AI application in these systems.

JAE-YOUNG PYUN received the B.S. degree from Chosun University, in 1997, the M.S. degree from Chonnam University, in 1999, and the Ph.D. degree in electronics engineering from Korea University, South Korea, in 2003. From 2003 to 2004, he was with Samsung Electronics, where he was involved in the research and development of mobile phone communication systems. He joined the Department of Information and Communication Engineering, Chosun University, in 2004, where he is currently a Professor. His research interests include the IoT protocols, platforms, and applications. Specifically, he conducts research on indoor positioning systems (IPSs), real-time location systems (RTLSs), and the IoT platforms combined with machine and deep learning.